Research article

Journal of Applied Toxicology

Received: 15 October 2015, Revised: 3 December 2015, Accepted: 4 January 2016 Published online in Wiley Online Library

(wileyonlinelibrary.com) DOI 10.1002/jat.3299

Differential cytotoxicity of copper ferrite nanoparticles in different human cells

Javed Ahmad[a,b], Hisham A. Alhadlaq[c,d], Aws Alshamsan[c,e], Maqsood A. Siddiqui[a,b], Quaiser Saquib[a,b], Shams T. Khan[a,b], Rizwan Wahab[a,b], Abdulaziz A. Al-Khedhairy[a], Javed Musarrat[f], Mohd Javed Akhtar[c] and Maqusood Ahamed[c]*

Abstract: Copper ferrite nanoparticles (NPs) have the potential to be applied in biomedical fields such as cell labeling and hyperthermia. However, there is a lack of information concerning the toxicity of copper ferrite NPs. We explored the cytotoxic potential of copper ferrite NPs in human lung (A549) and liver (HepG2) cells. Copper ferrite NPs were crystalline and almost spherically shaped with an average diameter of 35 nm. Copper ferrite NPs induced dose-dependent cytotoxicity in both types of cells, evident by 3-(4,5-dimethylthiazol-2-yl)-2,5-diphenyltetrazoliumbromide and neutral red uptake assays. However, we observed a quite different susceptibility in the two kinds of cells regarding toxicity of copper ferrite NPs. Particularly, A549 cells showed higher susceptibility against copper ferrite NP exposure than those of HepG2 cells. Loss of mitochondrial membrane potential due to copper ferrite NP exposure was observed. The mRNA level as well as activity of caspase-3 enzyme was higher in cells exposed to copper ferrite NPs. Cellular redox status was disturbed as indicated by induction of reactive oxygen species (oxidant) generation and depletion of the glutathione (antioxidant) level. Moreover, cytotoxicity induced by copper ferrite NPs was efficiently prevented by *N*-acetylcysteine treatment, which suggests that reactive oxygen species generation might be one of the possible mechanisms of cytotoxicity caused by copper ferrite NPs. To the best of our knowledge, this is the first report showing the cytotoxic potential of copper ferrite NPs in human cells. This study warrants further investigation to explore the mechanisms of differential toxicity of copper ferrite NPs in different types of cells. Copyright © 2016 John Wiley & Sons, Ltd.

Keywords: copper ferrite NPs; cytotoxicity; A549 cells; HepG2 cells; Oxidative stress

Introduction

Nanotechnology has now been recognized as a promising field that provides opportunity for the development of nanostructured materials (1–100 nm size) with unique physicochemical properties. Magnetic nanoparticles (NPs) are used in biomedical applications because of their interesting properties such as superparamagnetic behavior, high surface-to-volume ratio and external magnetic force (Al-Qubaisi *et al.,* 2013; Sahoo *et al.,* 2014). Spinel ferrite XFe_2O_4 (where X = Cu, Ni, Zn, Mg, Co., etc.) NPs are a very important class of magnetic materials because of their unique optical, electronic and magnetic properties. Spinel ferrite NPs have a high permeability, good saturation magnetization and no preferred direction of magnetization (Sun *et al.,* 2008). They are magnetically soft, being easily magnetized and demagnetized, and electrically insulating. Copper ferrite NP is one of the important spinel ferrites because it exhibits phase transition, changes semiconducting property, shows electrical switching and tetragonality variation under various situations in addition to interesting magnetic and electrical properties with great thermal and chemical stabilities (Rashad *et al.,* 2012; Sartale *et al.,* 2003). It is utilized in the wide range of applications, including gas sensing, catalytic applications, Li ion batteries, high density magneto-optic recording devices, color imaging, bioprocessing, magnetic refrigeration and ferrofluids (Rashad *et al.,* 2012; Roy and Ghose, 2006; Sun *et al.,* 2007). Copper ferrite NPs also possess a great potential for their application in biomedical fields such as diagnostic imaging, cell labeling, site-directed drug delivery and hyperthermia. However, using copper ferrite NPs for biomedical purposes remains a challenge due to lack of our understanding on the biological response of these NPs at the cellular and molecular level.

The toxicity assessment of spinel ferrite NPs is gaining momentum. Saquib *et al.* (2013 suggested that zinc ferrite ($ZnFe_2O_4$) NPs trigger apoptosis and/or necrosis in human amnion epithelial (WISH) cells through the mitochondria-dependent intrinsic apoptotic pathway. Horev-Azaria *et al.* (2013 reported that copper ferrite NPs induced toxicity to different cell lines (e.g., A549, HepG2, NCIH441, MDCK,

*Correspondence to: Dr. Maqusood Ahamed, Assistant Professor, King Abdullah Institute for Nanotechnology, King Saud University, Riyadh 11451, Saudi Arabia. E-mail: maqusood@gmail.com

[a]Department of Zoology, College of Science, King Saud University, Riyadh, Saudi Arabia

[b]Al-Jeraisy Chair for DNA Research, King Saud University, Riyadh, Saudi Arabia

[c]King Abdullah Institute for Nanotechnology, King Saud University, Riyadh, Saudi Arabia

[d]Department of Physics and Astronomy, College of Science, King Saud University, Riyadh, Saudi Arabia

[e]Nanomedicine Research Unit, Department of Pharmaceutics, College of Pharmacy, King Saud University, Riyadh, Saudi Arabia

[f]Department of Agricultural Microbiology, Faculty of Agricultural Sciences, Aligarh Muslim University, Aligarh, India

Caco-2/TC7 and TK6 cells) and rat lung slices. Cobalt ferrite and zinc ferrite NPs have also been reported to induce chromosomal aberration in the meristematic root cells of sunflowers (Vochita *et al.,* 2012). Another study suggested that cytotoxicity of nickel ferrite NPs arises in part from their effect on cellular energy metabolism, as nickel ferrite NPs decrease mitochondrial function (Tomitaka *et al.,* 2009). Our earlier reports also observed that nickel ferrite and zinc ferrite NPs induced cytotoxicity in different human cells (Ahamed *et al.,* 2011, 2015; Alhadlaq *et al.,* 2015). To the best of our knowledge, there are no studies on the toxicity of copper ferrite NPs at the cellular and molecular level.

Oxidative stress due to excessive production of reactive oxygen species (ROS) has been proposed as one of the underlying mechanisms of NP toxicity. ROS are physiologically necessary and has the potential to damage cell macromolecules. ROS may contribute to tissue damage in many pathophysiological conditions and participate in several cellular events, including signal transduction, proliferative response, gene expression and protein redox regulation (Dalle-Donne *et al.,* 2007; Lee *et al.,* 2014). It is manifested in the activation of ROS, followed by a proinflammatory response and DNA damage leading to mutagenesis and apoptosis (Finkel and Holbrook, 2000).

One can be exposed to NPs through the skin, lung or by ingestion (Oberdorster *et al.,* 2005). Therefore, it is crucial to explore the cellular response of copper ferrite NPs in relevant human cell lines. We have selected two well-characterized cell lines, i.e., human lung (A549) and liver (HepG2) cells, as models to explore toxic response of copper ferrite NPs. The A549 cells were used because the lung represents the main exposure route for workers employed in the production and handling of NPs as well as environmental exposure to the general population (Yang *et al.,* 2012). The A549 cell line has widely been used in toxicity studies (Barillet *et al.,* 2010; Foldbjerg *et al.,* 2011; Hanagata *et al.,* 2011). The HepG2 cells were utilized because liver is a primary site of NP accumulation after they gain entry into the body through any of the possible routes of exposure (Kim *et al.,* 2008). Studies reported that NPs, when ingested to mice, accumulate in the liver via blood circulation and induce liver toxicity (Johnston *et al.,* 2009; Wang *et al.,* 2008). The HepG2 cell line is a classical hepatic model used to test compounds that are potentially toxic or affect hepatocyte functions (Piret *et al.,* 2012; Siddiqui *et al.,* 2013). This study was designed to investigate how copper ferrite NPs interact with two different human cells (A549 and HepG2) to understand the interaction of this NP on cellular systems. In addition, ROS, glutathione (GSH), mitochondrial membrane potential (MMP) and cell cycle and caspase activity were used to explore potential mechanisms through which copper ferrite NPs induced toxicity to these cells. This preliminary study provides insight into the differential cytotoxicity of copper ferrite NPs to different human cells.

Materials and methods

Chemicals and reagents

Dulbecco's modified Eagle's medium (DMEM), penicillin–streptomycin and fetal bovine serum (FBS) were purchased from Invitrogen (Carlsbad, CA, USA). The 3-(4,5-dimethylthiazol-2-yl)-2,5-diphenyltetrazoliumbromide (MTT), 3-amino-7-dimethylamino-2-methyl-phenazine hydrochloride (neutral red), *N*-acetylcysteine (NAC), rhodamine-123 (Rh^{123}) and 2′,7′-dichlorofluorescin diacetate (DCFH-DA) were bought from Sigma-Aldrich (St. Louis, MO, USA). Caspase-3 and caspase-9 enzyme assay kits were obtained from Bio-Vision Inc. (Milpitas, CA, USA). Other chemicals were of analytical grade and bought from the available commercial sources.

Copper ferrite nanoparticles

Dry nanopowder of copper ferrite or copper iron oxide (product no. 641723, $<$ 100 nm particle size, $>$ 98.5% trace metals basis) was obtained from Sigma-Aldrich. Before toxicity assays, we characterized the copper ferrite NPs in our laboratory.

Copper ferrite nanoparticle characterization

Crystalline nature of copper ferrite NPs was measured by X-ray diffraction (XRD) equipment. The XRD pattern of nanopowder was acquired at room temperature with the help of a PANalytical X'Pert X-ray diffractometer (Almelo, The Netherland) equipped with an Ni filter using Cu Kα ($\lambda = 1.54056$ Å) radiations as an X-ray source. Structural characterization of copper ferrite NPs was done by field emission transmission electron microscopy (FETEM, JEM-2100F; JEOL Inc., Tokyo, Japan) at an accelerating voltage of 200 kV. In brief, 1 mg ml^{-1} suspension of copper ferrite NPs was prepared in deionized water. Then suspension was sonicated at room temperature for 15 min at 40 W to avoid NP agglomeration. A stock suspension was diluted to appropriate working solutions. Further, a drop of aqueous suspension of copper ferrite NPs was poured on to a carbon-coated copper grid, air-dried and FETEM measurements were performed. Elemental composition of copper ferrite NPs was done by energy dispersive X-ray spectroscopy (EDS).

The behavior of copper ferrite NPs in aqueous state (e.g., water and culture medium) was evaluated by dynamic light scattering (DLS) (Nano-ZetaSizer-HT, Malvern, UK) as reported elsewhere (Murdock *et al.,* 2008). Briefly, copper ferrite nanopowder was suspended in deionized water, and before and after exposure to cell media (DMEM +10% FBS) at the concentration of 100 μg ml^{-1}. This suspension was sonicated at room temperature for 15 min at 40 W and the DLS measurements were performed. We have utilized the concentration of 100 μg ml^{-1} in the DLS study because this was the highest dosage level employed in toxicity assays.

Cell culture and treatment of nanoparticles

The A549 and HepG2 cells were obtained from the American Type Culture Collection (Manassas, VA, USA). Cells were cultured in DMEM medium supplemented with 10% FBS and 100 U ml^{-1} penicillin–streptomycin at 5% CO_2 and 37°C. At 85% confluence, cells were harvested using 0.25% trypsin and were subcultured for further experiments. Cells were allowed to attach on the surface of the culture flask for 24 h before the NP exposure. Dry powder of copper ferrite NPs was suspended in DMEM medium at a concentration of 1 mg ml^{-1} and diluted to the appropriate dosages (10–100 μg ml^{-1}). The different concentrations of NPs were then sonicated at room temperature for 15 min at 40 W to avoid agglomeration of NPs before exposure to cells. In some experiments, cells were pre-exposed for 1 h with 10 mM of NAC before 24 h co-exposure with or without copper ferrite NPs. Cells not exposed to copper ferrite NPs served as controls in each experiment. The selection of the 10–100 μg ml^{-1} dosage range of copper ferrite NPs was based on a preliminary dose–response study (data not shown).

Journal of Applied Toxicology

MTT assay

Cell viability was done following the method as described by Mossman (1983 with few changes (Ahamed *et al.,* 2011). This assay evaluates the mitochondrial function by determining the ability of living cells to reduce MTT into a blue formazon product. Briefly, 1×10^4 cells per well were seeded in 96-well plates and exposed to different concentrations of copper ferrite NPs (10–100 $\mu g\ ml^{-1}$) for 24 h. After the treatment time was completed, culture medium was taken from each well to avoid interference of NPs and replaced with new medium containing the MTT solution in an amount equal to 10% of culture volume and incubated for 3 h at 37°C until a purple-colored formazan product developed. The resulting formazan product was dissolved in acidified isopropanol. Then, 96-well plate was centrifuged at 2300 g for 5 min to settle down the remaining NPs. Furthermore, 100 µl supernatant was transferred to a new 96-well plate, and the absorbance was taken at 570 nm utilizing a microplate reader (Synergy-HT; BioTek, Winooski, VT).

Neutral red uptake assay

The neutral red uptake (NRU) assay was performed following the procedure as described by Borenfreund and Puerner (1984 with some modifications (Ahamed *et al.,* 2011). In brief, 1×10^4 cells per well were seeded in to 96-well plates and exposed to different concentrations of copper ferrite NPs (10–100 $\mu g\ ml^{-1}$) for 24 h. At the end of the exposure time, test solution was aspirated and cells were washed with phosphate-buffered saline (PBS) twice before being incubated for 3 h in medium supplemented with neutral red (50 $\mu g\ ml^{-1}$). The medium was washed off rapidly with a solution containing 0.5% formaldehyde and 1% calcium chloride. The cells were then incubated for a further 20 min at 37°C in a mixture of acetic acid (1%) and ethanol (50%) to extract the dye. The 96-well plate was then centrifuged at 2300 *g* for 5 min to settle down the NPs, if present in the solution. Following this 100 µl supernatant was transferred to new 96-well plate and the absorbance was measured at 540 nm using the microplate reader (Synergy-HT; BioTek).

Reactive oxygen species assay

Intracellular ROS generation after the treatment of copper ferrite NPs was evaluated using DCFH-DA as reported by Wang and Joseph (1999 with a few changes, as described in our previous publication (Siddiqui *et al.,* 2013). The ROS level was measured using two methods (fluorometric quantitative assay by micro-plate reader and cell imaging by fluorescence microscopy). For the fluorometric assay, 1×10^4 cells per well were seeded in to 96-well black-bottomed culture plates and allowed to attach on the surface for 24 h in a CO_2 incubator at 37°C. Further, cells were treated with copper ferrite NPs for 24 h. After the exposure was completed, cells were washed twice with Hanks' balanced salt solution before being incubated in 1 ml of working solution of DCFH-DA for 30 min at 37°C. After this, cells were lysed in alkaline solution and centrifuged at 2300 *g* for 10 min. A 200 µl supernatant was transferred in to a new 96-well plate, and fluorescence was measured at 485 nm excitation and 520 nm emissions utilizing the microplate reader (Synergy-HT; BioTek). The values were presented as a percentage of fluorescence intensity relative to the controls.

A parallel set of cells (5×10^4 cells per well in a 24-well transparent plate) were assayed for intracellular fluorescence using a fluorescence microscope (Olympus CKX 41, Tokyo, Japan), with images captured at the magnification of 20×.

Cell extract preparation

Crude cell extract were prepared according to the protocol described in our earlier work (Ahmad *et al.,* 2012). The cell extract were used for GSH and caspase-3 enzyme assays. In brief, cells were cultured in a 75 cm^2 culture flask and treated with copper ferrite NPs for 24 h. After the exposure was completed, cells were harvested in ice-cold PBS by scraping and washed with PBS at 4°C. The cell pellets were then lysed in cell lysis buffer (1 × 20 mM Tris–HCl [pH 7.5, 150 mM NaCl, 1 mM Na_2EDTA, 1% Triton, 2.5 mM sodium pyrophosphate). Following centrifugation (15 000 *g* for 10 min at 4°C) the cell extract (supernatant) was stored in ice for assays.

Glutathione assay

Intracellular GSH content was estimated utilizing Ellman's method (1959). In brief, a mixture of 0.1 ml of crude cell extract and 0.9 ml of 5% trichloroacetic acid was centrifuged at 2300 *g* for 15 min. After that, 0.5 ml of the supernatant was added to 1.5 ml of 0.01% 5,5′-dithiobis-(2-nitrobenzoic acid and the reaction was monitored at 412 nm. The content of GSH was presented in terms of nmol mg^{-1} protein.

Mitochondrial membrane potential assay

The MMP was estimated using the method of Zhang *et al.* (2011) with a few changes (Ahamed and Alhadlaq, 2014). Briefly, cells (5×10^4 cells per well) were exposed to copper ferrite NPs for 24 h. After completion of the exposure time, cells were harvested and washed twice with PBS. Then, cells were treated with 10 $\mu g\ ml^{-1}$ Rh^{123} fluorescent dye for 1 h at 37°C in the dark. Furthermore, cells were washed twice with PBS then the fluorescence intensity of Rh^{123} dye was determined using upright fluorescence microscope (Olympus CKX 41) by grabbing the images at 20× magnification.

A parallel set of cells (1×10^4 cells per well) in a 96-well plate were analyzed for quantification of Rh^{123} using the microplate reader (Synergy-HT; BioTek).

Flow cytometric analysis of cell cycle progression

Cells treated with a concentration of 100 $\mu g\ ml^{-1}$ copper ferrite NPs for 24 h were harvested and centrifuged at 1000 *g* for 4 min. Pellets were resuspended in 500 µl of PBS. Cells were fixed with an equal volume of chilled 70% ice-cold ethanol, and incubated at 4°C for 1 h. After two successive washes with PBS at 1000 g for 4 min, cell pellets were resuspended in PBS and stained with 50 µg propidium iodide ml^{-1} containing 0.1% Triton X-100 and 0.5 mg ml^{-1} RNAase A for 1 h at 30°C in the dark. Fluorescence of the propidium iodide was measured by flow cytometry using a Beckman Coulter flow cytometer (Coulter Epics XL/Xl-MCL, Miami, FL, USA) through a FL-4 filter (585 nm) and 10 000 events were acquired (Darzynkiewicz *et al.*, 1992). The data were analyzed by Coulter Epics XL/XL-MCL, System II Software, Version 3.0. Cell debris characterized by a low forward/side scatter was excluded from the analysis.

Quantitative assay of caspase-3 gene by real-time polymerase chain reaction

Cells were cultured in six-well plates and treated with copper ferrite NPs at the concentration of 50 and 100 μg ml^{-1} for 24 h. After the completion of exposure time, total RNA was extracted by Qiagen RNeasy mini Kit (Valencia, CA, USA) according to the manufacturer's protocol. The RNA content was estimated using the Nanodrop 8000 spectrophotometer (Thermo-Scientific, Wilmington, DE, USA), and the integrity of RNA was visualized on a 1% agarose gel using the gel documentation system (Universal Hood II; BioRad, Hercules, CA, USA). The first strand of cDNA was synthesized from 1 μg of total RNA by the reverse transcriptase using M-MLV (Promega, Madison, WI, USA) and oligo(dT) primers (Promega) according to the manufacturer's instructions. Quantitative real-time polymerase chain reaction (PCR) was performed by the QuantiTect SYBR Green PCR kit (Qiagen) using the ABI PRISM 7900HT Sequence Detection System (Applied Biosystems, Foster City, CA, USA). Two microliters of template cDNA was added to the final volume of 20 μl of the reaction mixture. Real-time PCR cycle parameters included 10 min at 95°C followed by 40 cycles involving denaturation at 95°C for 15 s, annealing at 60°C for 20 s and elongation at 72°C for 20 s. The sequences of the specific sets of primer for caspase-3 and β-actin are reported in our earlier work (Ahamed *et al.,* 2011). Expressions of selected genes were normalized to the β-actin gene, which was used as controls.

Caspase-3 enzyme assay

Caspase-3 enzyme activity was evaluated in exposed and control cells using Bio-Vision colorimetric assay kits. Preparation of cell extract is as reported above. This assay is based on the principle that activated caspases in apoptotic cells cleave the synthetic substrates to release free chromophore p-nitroanilide (pNA), which is measured at 405 nm. The pNA was generated after specific action of the caspase-3 enzyme on tertrapeptide substrates DEVD-pNA (Ahamed *et al.,* 2011; Berasain *et al.,* 2005). In brief, the reaction mixture consisted of 50 μm of cell extract protein (as prepared above), 50 μl of 2 × reaction buffer (containing 10 mM dithiothreitol) and 5 μl of 4 mM DEVD-pNA substrate in a total volume of 105 μl. The reaction mixture was incubated at 37°C for 1 h and absorbance of the final product was estimated utilizing the microplate reader (Synergy-HT; BioTek) at 405 nm according to manufacturer's instructions.

Protein assay

Protein content was estimated by the Bradford method (1976) using bovine serum albumin as the standard.

Statistical analysis

Statistical significance was measured by one-way analysis of variance followed by Dunnett's multiple comparison tests. Significance was ascribed at $P < 0.05$.

Results

Characterization

The XRD pattern of copper ferrite NPs is shown in Fig. 1. This image demonstrates the sharp well defined peaks corresponding to the planes of (111), (202), (220), (113), (311), (222), (400), (224), (422), (511), (440) and (622) indicating spinel structure of copper ferrite NPs without any impure phase. All the diffraction peaks in the XRD pattern can be indexed to those of the tetragonal structure of copper ferrite according to JCPDS file no. 34–0425. The crystallite size (*d*) has been estimated from the XRD pattern using the Scherrer's equation (Patterson, 1939).

$$d = \frac{K\lambda}{\beta \mathrm{Cos}\theta}$$

where K = 0.9 is the shape factor, λ is the X-ray wavelength of Cu Kα radiation (1.54 Å), θ is the Bragg diffraction angle and β is the broadening of diffraction line measured at half of its maximum intensity (in radians). The average crystallite size of nickel ferrite NPs was found to be about 34.87 nm. Shape and size of copper ferrite NPs were characterized by FETEM. Figure 2 (A) shows the FETEM image of copper ferrite NPs. This image exhibits that the majority of the particles were spherical shaped with smooth surfaces. High-resolution TEM image suggested the crystalline nature of copper ferrite NPs (Fig. 2B). TEM average diameter was calculated from measuring over 110 particles in random fields of view. The average TEM size of copper ferrite NPs was found to be approximately 35.32 nm (range 5–65 nm) supporting the XRD data. Elemental composition of copper ferrite NPs analyzed by EDS was presented in Fig. 2(C). The EDS pattern suggests that no elemental impurities present in copper ferrite NPs. Figure 2(D) represents the frequency of size distribution of copper ferrite NPs.

DLS characterization of copper ferrite NPs was done in an aqueous state. Hydrodynamic size and zeta potential of copper ferrite NPs in deionized water and culture media (before and after exposure to cells) is given in Table 1.

Cell viability and morphology of cells

HepG2 and A549 cells were treated to different dosages (10–100 μg ml^{-1}) of copper ferrite NPs for 24 h and cell viability was examined by the MTT and NRU assays. These assays have shown that copper ferrite NPs induced dose-dependent cytotoxicity in both types of cells. MTT results showed that viability of HepG2 cells was decreased to 83, 72, 63 and 54%, while A549 cell viability

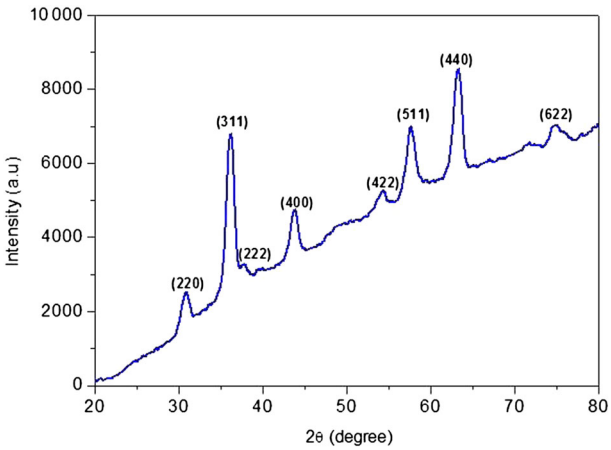

Figure 1. X-ray diffraction pattern of copper ferrite nanoparticles.

Journal of AppliedToxicology

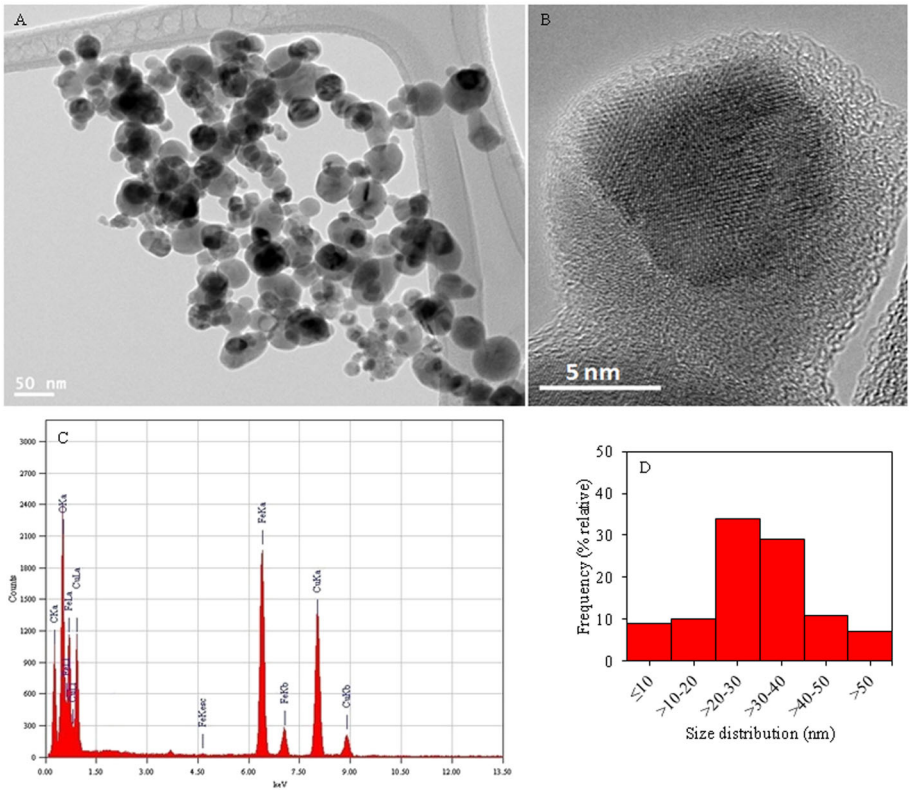

Figure 2. Electron microscopy characterization of copper ferrite nanoparticles. (A) Field emission transmission electron microscopy image. (B) High-resolution field emission transmission electron microscopy image. (C) Elemental composition analysis. (D) Size distribution of copper ferrite nanoparticles.

reduction was 78, 69, 51 and 40% at the concentrations of 10, 25, 50 and 100 $\mu g\,ml^{-1}$, respectively ($P < 0.05$ for each) (Fig. 2A). Figure 3(B) shows the results of cell viability obtained by NRU assay. NRU results were in agreement with MTT data.

Interestingly, we observed that A549 cells were more vulnerable to copper ferrite NP exposure as compared to HepG2 cells. At higher concentrations (50 and 100 $\mu g\,ml^{-1}$), copper ferrite NPs reduction in cell viability in A549 cells was significantly higher than those of HepG2 cells (63 and 54% cell viability reduction for HepG2 vs. 51 and 40% cell viability reduction in A549).

We further assessed the cell morphology following exposure to copper ferrite NPs using a Leica phase contrast microscope. Figure 3(C) shows the comparative morphologies of HepG2 and A549 cells after copper ferrite NP exposure. A significant lowering of cell density and rounding of cells were observed due to copper ferrite NP exposure and supporting the cell viability data.

Table 1. Dynamic light scattering characterization of copper ferrite nanoparticles

	Deionized water	Culture media: before exposure to cells	Culture media: after exposure to cells
Hydrodynamic size (nm)	437	387	311
Zeta potential (−mV)	16	19	21

Oxidative stress

ROS generation has been suggested as underlying mechanisms of nanoscale materials cytotoxicity (Lee *et al.,* 2014; Nel *et al.,* 2006; Xia *et al.,* 2006). We explored the potential of copper ferrite NPs to induce oxidative stress by measuring the ROS and GSH levels of HepG2 and A549 cells. Quantitative data demonstrated that copper ferrite NPs induced ROS generation in a dose-dependent manner in both cells ($P < 0.05$ for each) (Fig. 4A). Fluorescent microscopy image also revealed that copper ferrite NPs exposed cells express high-intensity green fluoresce of DCF dye (marker of ROS generation) as compared to control (Fig. 4B).

To investigate whether ROS generation plays a crucial role in cytotoxicity of copper ferrite NPs, cells were exposed to copper ferrite NPs in the presence of NAC. Results showed that NAC abolished almost fully the cytotoxic effect of copper ferrite NPs in both HepG2 and A549 cells (Fig. 4C). Antioxidant GSH levels were also lower in HepG2 and A549 cells after exposure to copper ferrite NPs (Fig. 4D).

Mitochondrial membrane potential

Earlier studies have shown that loss of MMP during the process of apoptotic cell death (Sharma *et al.,* 2012). We investigated the response of copper ferrite NPs on MMP in the HepG2 and A431 cells. Quantitative data showed that copper ferrite NPs induced MMP loss in a dose-dependent manner in both types of cells ($P < 0.05$) (Fig. 5A). Fluorescence microscopy results were also according to the quantitative data. The brightness of the red fluorescent intensity was decreased in cells treated with copper ferrite NPs that shows a significant loss of MMP (Fig. 5B).

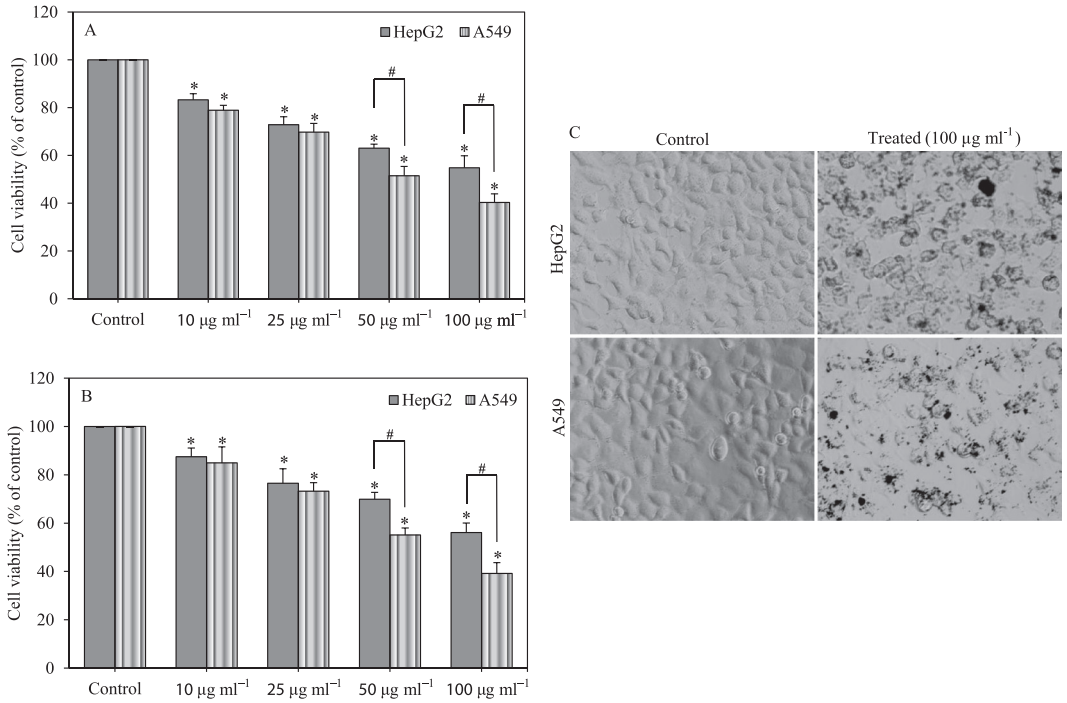

Figure 3. Cytotoxic response of copper ferrite nanoparticles in HepG2 and A549 cells. (A) MTT assay, (B) neutral red uptake assay and (C) cell morphology. Data represented are mean ± SD of three identical experiments made in three replicate. *Significant difference as compared to the controls ($P < 0.05$). #Significant difference in cytotoxicity between HepG2 and A549 cells ($P < 0.05$).

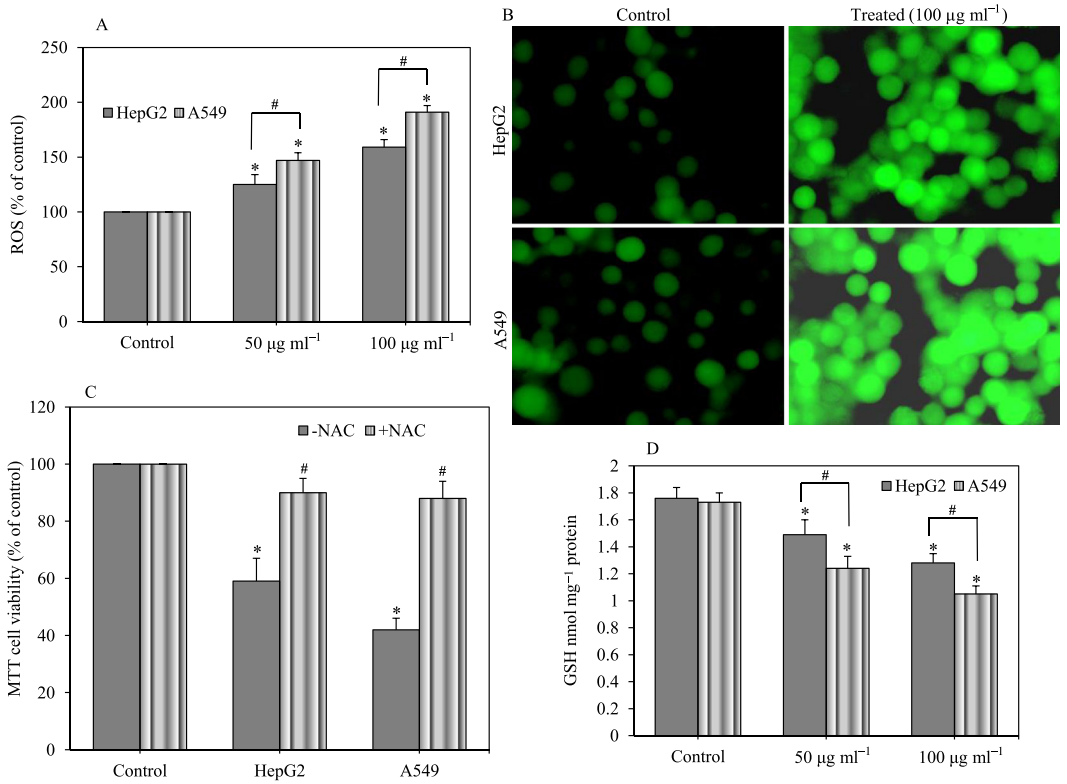

Figure 4. Induction of oxidative stress by copper ferrite nanoparticles in HepG2 and A549 cells. (A) Percentage change in ROS level. (B) Fluorescence microscopy image of ROS generation. (C) MTT cell viability against copper ferrite nanoparticle exposure in the presence of antioxidant NAC. (D) GSH level. Data represented are mean ± SD of three identical experiments made in three replicate. *Significant difference as compared to the controls ($P < 0.05$). #Significant difference in oxidative stress between HepG2 and A549 cells ($P < 0.05$). GSH, glutathione; NAC, *N*-acetyl cysteine; ROS, reactive oxygen species.

Journal of AppliedToxicology

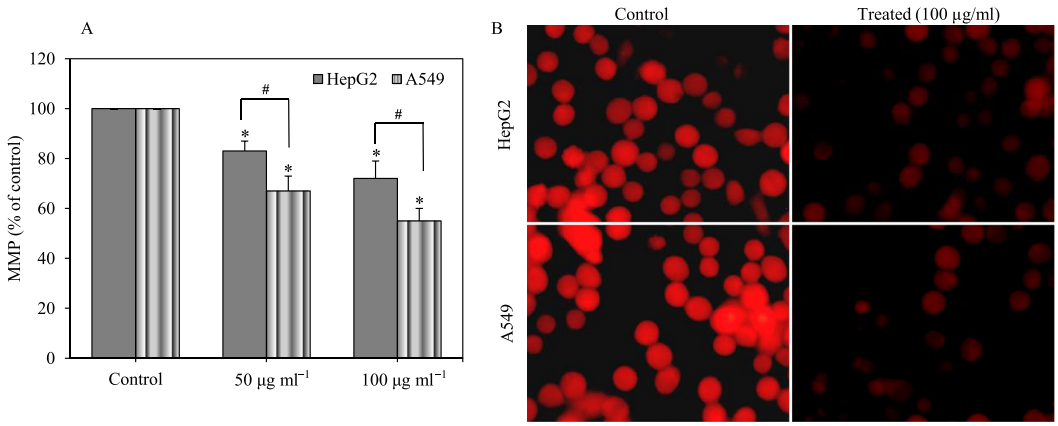

Figure 5. MMP loss due to copper ferrite nanoparticle exposure in HepG2 and A549 cells. (A) Percentage change in MMP level. (B) Fluorescence microscopy image showing MMP loss. Data represented are mean ± SD of three identical experiments made in three replicate. *Statistically significant difference as compared to control ($P < 0.05$). #Significant difference in MMP loss between HepG2 and A549 cells ($P < 0.05$). MMP, mitochondrial membrane potential.

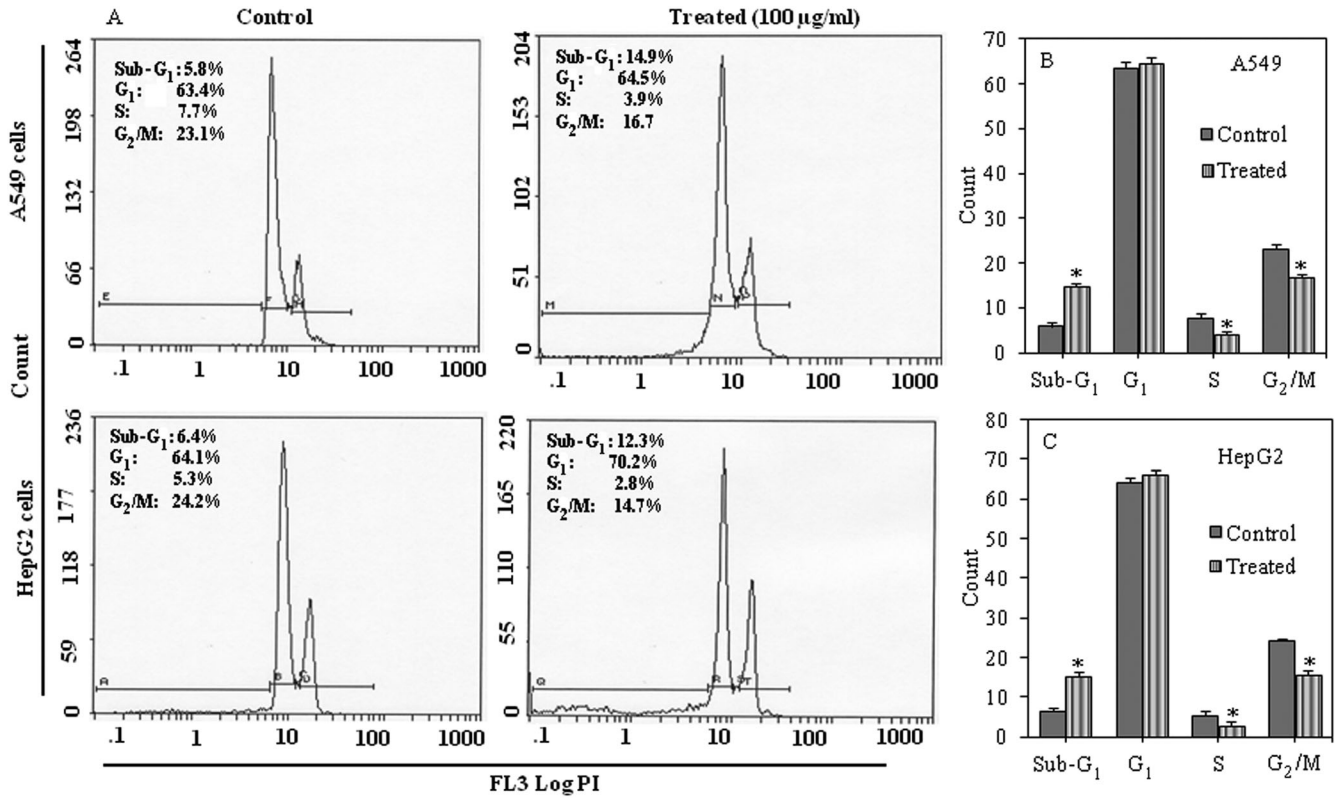

Figure 6. Cell cycle analysis of A549 and HepG2 cells after copper ferrite nanoparticle exposure. (A) Representative flow cytometric images showing changes in the progression of cell cycle. The G_1, S and G_2/M in each micrograph represent the percentage of cells present in normal phases of cell cycle whereas sub-G_1 represents percentage of cells that undergone apoptosis. (B,C) Each histogram represents mean ± SD values of different phases of cell cycle obtained from three identical experiments made in three replicate. *Statistically significant difference as compared to control ($P < 0.05$).

Cell cycle

ROS generation in copper ferrite NP-treated cells indicated the possibility of DNA damage and apoptosis where the early effect will be evidenced in cell cycle progression. Cells with damaged DNA will accumulate in gap1 (G_1), DNA synthesis (S) or in gap2/mitosis (G_2/M) phase. Cells with irreversible damage will undergo apoptosis, giving rise to accumulation of cells in sub-G_1 phase (Ishikawa *et al.,* 2006). Thus, our toxicity studies were further extended to cell cycle analysis to detect parameters such as apoptosis. Our flow-cytometric analysis of cell cycle revealed the induction of apoptosis in both A549 and HepG2 cells upon treatment with copper ferrite NPs (Fig. 6A). In A549 cells, copper ferrite NPs at the highest concentration of 100 μg ml^{-1} resulted in the appearance of a significant 14.9% cells in the sub-G_1 phase in treated cells as compared to the 5.8% in the control group (Fig. 6B). Similarly, in HepG2 cells 12.3% cells were accumulated in exposed cells than those of 6.4% of control (Fig. 6C). A significant decline in the S phase and G_2/M phase was also evident in both types of cells.

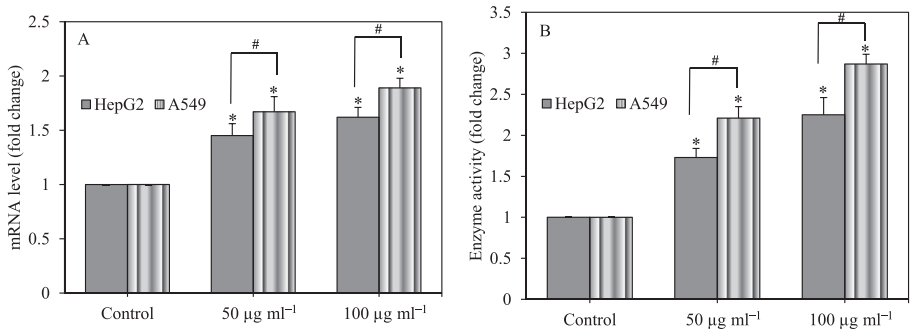

Figure 7. Effect of copper ferrite nanoparticles on caspase-3. (A) Regulation of mRNA levels of caspase-3 gene. (B) Activity of caspase-3 enzyme. Data represented are mean ± SD of three identical experiments made in three replicates. *Significant difference as compared to the controls ($P < 0.05$). #Significant difference in caspase-3 gene and enzyme between HepG2 and A549 cells ($P < 0.05$).

Caspase-3 enzyme

Caspases are activated during apoptosis in many cells and are known to play a vital role in both the initiation and execution of apoptosis. It was reported that caspase-3 is essential for cellular DNA damage and apoptosis (Salvesen, 2002). We studied the effect of copper ferrite NPs on transcriptional and translational level of caspase-3 gene. Quantitative real-time PCR data showed that the mRNA level of caspase-3 gene was higher in HepG2 and A549 cells treated with copper ferrite NP-treated cells as compared to the control ($P < 0.05$) (Fig. 7A). In agreement with mRNA results, the activity of the caspase-3 enzyme was also higher in both HepG2 and A549 cells exposed to copper ferrite NPs than those to control (Fig. 7B). We also noticed that the effect of copper ferrite NPs on caspase-3 enzyme was significantly higher in A549 cells than HepG2 cells.

Altogether, our results highlighted that at higher concentrations A549 cells showed more susceptibility to copper ferrite NPs as compared to HepG2 cells terms of cell viability, oxidative stress, MMP and caspase-3 enzyme. However, underlying mechanisms of cytotoxicity look similar in both types of cells.

Discussion

Physical and chemical properties play a major role in the toxicity of NPs (Murdock *et al.,* 2008; Warheit, 2008). Shape, size, surface morphology and chemical composition could be the important characteristics of NPs that may influence the cellular response of NPs. After incubation in distilled water and complete cell culture media (DMEM +10% FBS), the diameter of copper ferrite NPs of 35 nm increased to 437 and 387 nm, respectively, determined by the DLS technique (Table 1). The size distributions of particles aqueous media showed larger values than the particle size of nanopowder measured by TEM. This shows that the copper ferrite NPs formed agglomerates in the culture medium, which were about 10–15 times higher than the primary particle size (35 nm). These data are supported by others (Bai *et al.,* 2009; Sharma *et al.,* 2009) as well as our earlier published work (Ahmad *et al.,* 2012; Akhtar *et al.,* 2012). DLS measures Brownian motion and subsequent size distribution of an ensemble collection of NPs in aqueous suspension gives a mean hydrodynamic diameter that is usually larger than the TEM diameter because it represents a dried layer of NPs on a TEM grid. During DLS measurement, there is a tendency of NPs to agglomerate in aqueous state thereby giving the size of clustered particles rather than individual particles (Sharma *et al.,* 2012). Moreover, the mean hydrodynamic size of copper ferrite in complete cell culture medium was found to be about slightly smaller than that in distilled water. A similar drop in the hydrodynamic size of NPs in culture medium was reported by other researchers (Ng *et al.,* 2011; Xia *et al.,* 2006), suggesting that salts and proteins could help the dispersion of NPs in aqueous environment. The tendency of particles to form aggregates also depends on the surface charge. The copper ferrite NP surface charge, measured as zeta potential was −16 and −19 mV for distilled water and cell culture media, respectively. Therefore, not only the size of the primary NPs but also the size of the secondary NPs could be used as a characteristic parameter to determine the toxic response of NPs (Avalos *et al.,* 2014; Kato, 2011).

After characterization, we performed a series of tests to examine the toxic response of copper ferrite NPs. Our results showed that copper ferrite NPs were cytotoxic to both the human lung A549 and human liver HepG2 cells. However, we observed a quite different behavior in the two kinds of cells regarding toxicity of tested copper ferrite NPs. In particular, we found A549 cells were more susceptible to copper ferrite NP exposure than HepG2 cells in terms of cell viability, cell morphology, oxidative stress, MMP and caspase-3 enzyme. Differential cytotoxicity of spinel ferrite NPs in different cell lines was also reported by other investigators. Pasukoniene *et al.* (2014 studied the effect of cobalt ferrite NPs on human pancreatic cancer cells (MiaPaCa2) and human ovarian cancer cells (A2780). They reported different cytotoxic response between MiaPaCa2 and A2780 cells. Particularly, A2780 cells were more sensitive to exposition to cobalt ferrite NPs than MiaPaCa2 cells.

We have employed more than one assay (MTT and NRU) to evaluate the cytotoxic response of copper ferrite NPs. These assays served as sensitive and integrated measures of cell integrity and inhibition of cell proliferation (Ahamed *et al.,* 2015; Avalos *et al.,* 2014; Sharma *et al.,* 2009). MTT and NRU assays have shown the damage of mitochondrial and lysosomal membranes, respectively (Ravi *et al.,* 2010). Our results are consistent with the observed low MMP and high sub-G_1 cell population during cell cycle progression in both cells (A549 and HepG2) exposed to copper ferrite NPs. Accumulation of cells in the sub-G_1 peak in treated cells suggested possible involvement of the apoptotic pathway, triggered by changes in mitochondrial and lysosomal activity (Nicoletti *et al.,* 1991; Ravi *et al.,* 2010). Mitochondrial events of apoptosis involve opening of a pore in the inner mitochondrial membrane, referred as mitochondrial permeability transition pore and loss of MMP (Kitsis and Molkentin, 2010). This is consistent with our results where copper ferrite NPs induced mitochondrial dysfunction (MTT reduction and MMP loss) in both cells. Opening of the mitochondrial permeability transition pore leads to mitochondrial

swelling and rupture of outer mitochondrial membrane. This subsequently induces release of apoptogens that likely engage the components of apoptosis machinery to enhance further the cell death (Kitsis and Molkentin, 2010). Damage to lysosomal membrane is known to release lysosome protease into intracellular spaces, which affects the neighbor cells, and triggers cell death due to apoptosis (Leist and Jaattela, 2001).

We further studied the caspase-3 gene (apoptotic marker) against copper ferrite NP exposure in A549 and HepG2 cells at the transcriptional level. Quantitative real-time PCR data demonstrated that copper ferrite NPs upregulated the mRNA level of caspase-3 gene in both cells. To confirm transcription data we also demonstrated that activity of caspase-3 enzyme was higher in copper ferrite NP-treated cells. We know that certain genes induce permeabilization of the outer mitochondrial membrane, which releases soluble proteins (e.g., cytochrome *c*) from the intermembrane space into the cytosol, where they promote caspase activation (Youle and Strasser, 2008). Cytochrome *c* binds to apoptosis protease activating factor-1 and forms an apoptosome complex. This complex binds to procaspase-9 and causes its activation. Once activated caspase-9 goes on to activate caspase-3 that cleaves substrates at aspartate residues and activation of this proteolytic activity appears to be an event in apoptosis (Timmer and Salvesen, 2007).

Oxidative stress has been suggested as a common mechanism through which NPs induced toxicity to cells (Lee *et al.,* 2014; Nel *et al.,* 2006). In this study, we observed that the ROS level was higher while the antioxidant GSH level was lower in both A549 and HepG2 cells against copper ferrite NP exposure. We also found that antioxidant NAC (ROS scavenger) efficiently prevented the cell viability reduction induced by copper ferrite NPs. These findings suggested that oxidative stress could be a primary cause of the cytotoxicity of copper ferrite NPs in both A549 and HepG2 cells. A number of previous studies have implicated the production of ROS in the cytotoxicity mediated by NPs (Foldbjerg *et al.,* 2011; Hussain *et al.,* 2005; Lee *et al.,* 2014; Xia *et al.,* 2006). The present results were in agreement with our earlier studies showing that magnetic NPs induce ROS-mediated cytotoxicity in various types of human cells (Ahamed *et al.,* 2011, 2015; Alhadlaq *et al.,* 2015).

In general metal and metal oxide NPs show some degree of ionization when they are suspended in aqueous state (water or culture media). However, the role of dissolved ions in the toxicity of NPs still needs extensive research. In this study, we did not examine the degree of ionization and its role in the toxicity of copper ferrite NPs. The role of ionization in the toxicity of copper ferrite NPs is a matter for further research. At this stage we demonstrated that copper ferrite NPs have the potential to induce cytotoxicity to human liver and lung cells.

Conclusions

We demonstrated that copper ferrite NPs caused cytotoxicity (MTT and NRU) to human lung (A549) and human liver (HepG2) cells in a dose-dependent manner in the dosage range of 10–100 $\mu g\ ml^{-1}$. Interestingly, we observed quite different behavior in the two kinds of cells regarding the toxicity of copper ferrite NPs. In particular, A549 cells showed higher susceptibility against copper ferrite NP exposure than those of HepG2 cells. MMP loss, upregulation of caspase-3 gene along with their higher enzymatic activity suggests apoptotic cell death due to copper ferrite NP exposure. Cellular redox status was disturbed indicated by induction of ROS (oxidant) generation and depletion of GSH (antioxidant). In addition, cytotoxicity induced by copper ferrite NPs was efficiently prevented by NAC treatment, which suggests that oxidative stress could be one of the possible mechanisms of cytotoxicity caused by copper ferrite NPs. Our data warranted future research on investigation of the underlying mechanisms of differential toxicity of copper ferrite NPs in cells of different origin.

Acknowledgments

The authors would like to extend their sincere appreciation to the Deanship of Scientific Research at King Saud University for its funding through research group no RG-1435-308.

Conflict of interest

The authors did not report any conflict of interest.

References

Ahamed M, Alhadlaq HA. 2014. Nickel nanoparticle-induced dose-dependent cyto-genotoxicity in human breast carcinoma MCF-7 cells. *Onco. Targets Ther.* **7**: 269–280.

Ahamed M, Akhtar MJ, Siddiqui MA, Ahmad J, Musarrat J, Al-Khedhairy AA, Alrokayan SA. 2011. Oxidative stress mediated apoptosis induced by nickel ferrite nanoparticles in cultured A549 cells. *Toxicology* **283**: 101–108.

Ahamed M, Akhtar MJ, Alhadlaq HA, Khan MAM, Alrokayan SA. 2015. Comparative cytotoxic response of nickel ferrite nanoparticles in human liver HepG2 and breast MFC-7 cancer cells. *Chemosphere* **135**: 278–288.

Ahmad J, Ahamed M, Akhtar MJ, Alrokayan SA, Siddiqui MA, Musarrat J, Al-Khedhairy AA. 2012. Apoptosis induction by amorphous silica nanoparticles mediated through reactive oxygen species generation in human liver cell line HepG2. *Toxicol. Appl. Pharmacol.* **259**: 160–168.

Akhtar MJ, Ahamed M, Kumar S, Ahmad J, Khan MAM, Ahmad J, Alrokayan SA. 2012. Zinc oxide nanoparticles selectively induces apoptosis in cancer cells through reactive oxygen species. *Int. J. Nanomed.* **7**: 845–857.

Alhadlaq HA, Akhtar MJ, Ahamed M. 2015. Zinc ferrite nanoparticle-induced cytotoxicity and oxidative stress in different human cells. *Cell Biosci.* **5**: 55.

Al-Qubaisi MS, Rasedee A, Flaifel MH, Ahmad SH, Hussein-Al-Ali S, Hussein MZ. 2013. Cytotoxicity of nickel zinc ferrite nanoparticles on cancer cells of epithelial origin. *Int. J. Nanomed.* **8**: 2497–2508.

Avalos A, Haza AI, Mateo D, Morales P. 2014. Cytotoxicity and ROS production of manufactured silver nanoparticles of different sizes in hepatoma and leukemia cells. *J. Appl. Toxicol.* **34**: 413–423.

Bai W, Zhang Z, Tian W, He X, Ma Y. 2009. Toxicity of zinc oxide nanoparticles to zebrafish embryo: A physicochemical study of toxicity mechanism. *J. Nanopart. Res.* **12**: 1645–1654.

Barillet S, Jugan ML, Laye M, Leconte Y, Herlin-Boime N, Reynaud C, Carriere M. 2010. In vitro evaluation of SiC nanoparticles impact on A549 pulmonary cells: cyto-, genotoxicity and oxidative stress. *Toxicol. Lett.* **198**: 324–330.

Berasain C, Garcia-Trevijano ER, Castillo J, Erroba E, Santamaria M, Lee DC. 2005. Novel role for amphiregulin in protection from liver injury. *J. Biol. Chem.* **280**: 19012–19020.

Borenfreund E, Puerner JA. 1984. A simple quantitative procedure using monolayer cultures for cytotoxicity assays. *J. Tissue Culture Method* **9**: 7–9.

Bradford MM. 1976. A rapid and sensitive method for the quantitation of microgram quantities of protein utilizing the principle of protein–dye binding. *Anal. Biochem.* **72**: 248–254.

Dalle-Donne I, Rossi R, Giustarini D, Colombo R, Milzani A. 2007. S-glutathionylation in protein redox regulation. *Free. Radic. Biol. Med.* **43**: 883–898.

Darzynkiewicz Z, Bruno S, Bino G. 1992. Features of apoptosis cells measured by flow cytometry. *Cytometry* **13**: 795–608.

Ellman GI. 1959. Tissue sulfhydryl groups. *Arch. Biochem. Biophys.* **82**: 70–77.

Finkel T, Holbrook NJ. 2000. Oxidants, oxidative stress and the biology of ageing. *Nature* **408**: 239–247.

Foldbjerg R, Dang DA, Autrup H. 2011. Cytotoxicity and genotoxicity of silver nanoparticles in the human lung cancer cell line, A549. *Arch. Toxicol.* **85**: 743–750.

Hanagata N, Zhuang F, Connolly S, Li J, Ogawa N, Xu M. 2011. Molecular responses of human lung epithelial cells to the toxicity of copper oxide nanoparticles inferred from whole genome expression analysis. *ACS Nano* **5**: 9326–9338.

Horev-Azaria L, Baldi G, Beno D, Bonacchi D, Golla-Schindler U, Kirkpatrick JC, Kolle S, Landsiedel R, Maimon O, Marche PN, Ponti J, Romano R, Rossi F, Sommer D, Uboldi C, Unger RE, Villiers C, Korenstein R. 2013. Predictive toxicology of cobalt ferrite nanoparticles: comparative in-vitro study of different cellular models using methods of knowledge discovery from data. *Part. Fibre Toxicol.* **10**: 32.

Hussain SM, Hess KL, Gearhart JM. 2005. In vitro toxicity of nanoparticles in BRL 3 A rat liver cells. *Toxicol. In Vitro* **19**: 975–983.

Ishikawa K, Ishii H, Saito T. 2006. DNA damage-dependent cell cycle checkpoints and genomic stability. *DNA Cell Biol.* **25**: 406–411.

Johnston HJ, Hutchison GR, Christensen FM, Peters S, Hankin S, Stone V. 2009. Identification of the mechanisms that drive the toxicity of TiO_2 particulates: the contribution of physicochemical characteristics. *Part. Fibre Toxicol.* **6**: 33.

Kato H 2011. In vitro assays: Tracking nanoparticles inside cells. *Nat. Nanotechnol.* **6**: 139–140.

Kim YS, Kim JS, Cho HS, Rha DS, Kim JM, Park JD, Choi BS, Lim R, Chang HK, Chung YH, Kwon IH, Jeong J, Han BS, Yu IJ. 2008. Twenty eight day oral toxicity, genotoxicity, and gender-related tissue distribution of silver nanoparticles in Sprague–Dawley rats. *Inhal. Toxicol.* **20**: 575–583.

Kitsis RN, Molkentin JD. 2010. Apoptotic cell death nixed by an ER-mitochondrial necrotic pathway. *Proc. Natl. Acad. Sci. USA* **107**: 9031–9032.

Lee YH, Cheng FY, Chiu HW, Tsai JC, Fang CY, Chen CW, Wang YJ. 2014. Cytotoxicity, oxidative stress, apoptosis and the autophagic effects of silver nanoparticles in mouse embryonic fibroblasts. *Biomaterials* **35**: 4706–4715.

Leist M, Jaattela M. 2001. Four deaths and a funeral: From caspases to alternative mechanisms. *Nat. Rev. Mol. Cell. Biol.* **2**: 589–598.

Mossman T 1983. Rapid colorimetric assay for cellular growth and survival: Application to proliferation and cytotoxicity assays. *J. Immunol. Methods* **65**: 55–63.

Murdock RC, Braydich-Stolle L, Schrand AM, Schlager JJ, Hussain SM. 2008. Characterization of nanomaterial dispersion in solution prior to in vitro exposure using dynamic light scattering technique. *Toxicol. Sci.* **101**: 239–253.

Nel A, Xia T, Madler L, Li N. 2006. Toxic potential of materials at the nanolevel. *Science* **311**: 622–627.

Ng KW, Khoo SK, Heng BC, Setyawati MI, Tan EC. 2011. The role of the tumor suppressor p53 pathway in the cellular DNA damage response to zinc oxide nanoparticles. *Biomaterials* **32**: 8218–8225.

Nicoletti I, Migliorati G, Pagliacci MC, Grignani F, Riccardi C. 1991. A rapid and simple method for measuring thymocyte apoptosis by propidium iodide staining and flow cytometry. *J. Immunol. Methods* **139**: 271–279.

Oberdorster G, Oberdorster E, Oberdorster J. 2005. Nanotoxicology: an emerging discipline evolving from studies of ultrafine particles. *Environ. Health Perspect.* **113**: 823–839.

Pasukoniene V, Mlynska A, Steponkiene S, Poderys V, Matulionytė M, Karabanovas V, Statkutė U, Purvinienė R, Kraśko JA, Jagminas A, Kurtinaitienė M, Strioga M, Rotomskis R. 2014. Accumulation and biological effects of cobalt ferrite nanoparticles in human pancreatic and ovarian cancer cells. *Medicina* **50**: 237–244.

Patterson AL. 1939. The Scherrer formula for X-ray particle size determination. *Phys. Rev.* **56**: 978–982.

Piret JP, Jacques D, Audinot JN, Mejia J, Boilan E. 2012. Copper (II) oxide nanoparticles penetrate into HepG2 cells, exert cytotoxicity via oxidative stress and induce pro-inflammatory response. *Nanoscale* **4**: 7168–7184.

Rashad MM, Mohamed RM, Ibrahim MA, Ismail EM, Abdel-Aal EA. 2012. Magnetic and catalytic properties of cubic copper ferrite nanopowders synthesized from secondary resources. *Adv. Powder Technol.* **23**: 315–323.

Ravi S, Chiruvella KK, Rajesh K, Prabhu V, Raghavan SC. 2010. 5-Isopropylidene-3-ethyl rhodamine induce growth inhibition followed by apoptosis in leukemia cells. *Eur. J. Med. Chem.* **45**: 2748–2752.

Roy S, Ghose J. 2006. Mossbauer study of nanocrystalline cubic $CuFe_2O_4$ synthesized by precipitation in polymer matrix. *J. Magn. Magn. Mater.* **307**: 32–37.

Sahoo B, Devi KS, Dutta S, Maiti TK, Pramanik P, Dhara D. 2014. Biocompatible mesoporous silica-coated superparamagnetic manganese ferrite nanoparticles for targeted drug delivery and MR imaging applications. *J. Colloid Interface Sci.* **431**: 31–41.

Salvesen GS. 2002. Caspases: opening the boxes and interpreting the arrows. *Cell Death Differ.* **9**: 3–5.

Saquib Q, Al-Khedhairy AA, Ahmad J, Siddiqui MA, Dwivedi S, Khan ST, Musarrat J. 2013. Zinc ferrite nanoparticles activate IL-1b, NFKB1, CCL21 and NOS2 signaling to induce mitochondrial dependent intrinsic apoptotic pathway in WISH cells. *Toxicol. Appl. Pharmacol.* **273**: 289–297.

Sartale SD, Lokhande CD, Muller M. 2003. Electrochemical synthesis of nanocrystalline $CuFe_2O_4$ thin films from non-aqueous (ethylene glycol) medium. *Mater. Chem. Phys.* **80**: 120–128.

Sharma V, Shukla RK, Saxena N, Parmar D, Das M. 2009. DNA damaging potential of zinc oxide nanoparticles in human epidermal cells. *Toxicol. Lett.* **185**: 211–218.

Sharma V, Anderson D, Dhawan A. 2012. Zinc oxide nanoparticles induce oxidative DNA damage and ROS-triggered mitochondria mediated apoptosis in human liver cells (HepG2). *Apoptosis* **17**(8): 852–870.

Siddiqui MA, Alhadlaq HA, Ahmad J, Al-Khedhairy AA, Musarrat J, Ahamed M. 2013. Copper oxide nanoparticles induced mitochondria mediated apoptosis in human hepatocarcinoma cells. *PLoS One* **8**: e69534.

Sun C, Lee JSH, Zhang M. 2008. Magnetic nanoparticles in MR imaging and drug delivery. *Adv. Drug Deliv. Rev.* **60**(11): 1252–1265.

Sun Z, Liu L, Jia DZ, Pan W. 2007. Simple synthesis of $CuFe_2O_4$ nanoparticles as gas-sensing materials. *Sens. Actuators B Chem.* **125**: 144–148.

Timmer JC, Salvesen GS. 2007. Caspase substrates. *Cell Death Differ.* **14**: 66–72.

Tomitaka A, Hirukawa A, Yamada T, Morishita S, Takemura Y. 2009. Biocompatibility of various ferrite nanoparticles evaluated by in vitro cytotoxicity assays using HeLa cells. *J. Magn. Magn. Mater.* **321**: 1482–1484.

Vochita G, Creanga D, Focanici-Ciurlica EL. 2012. Magnetic nanoparticle genetic impact on root tip cells of sunflower seedlings. *Water Air Soil Pollut.* **223**: 2541–2549.

Wang B, Feng W, Wang M, Wang T, Gu T, Zhu M, Ouyang H, Shi J, Zhang F, Zhao F, Chai Z, Wang H, Wang J. 2008. Acute toxicological impact of nano- and submicro-scaled zinc oxide powder on healthy adult mice. *J. Nanopart. Res.* **10**: 263–276.

Wang H, Joseph JA. 1999. Quantifying cellular oxidative stress by dichlorofluorescin assay using microplate reader. *Free Radic. Biol. Med.* **27**: 612–616.

Warheit DB. 2008. How meaningful are the results of nanotoxicity studies in the absence of adequate material characterization. *Toxicol. Sci.* **101**: 183–185.

Xia T, Kovochich M, Liong M, Mädler L, Gilbert B. 2006. Comparison of the mechanism of toxicity of zinc oxide and cerium oxide nanoparticles based on dissolution and oxidative stress properties. *ACS Nano* **2**: 2121–2134.

Yang X, Liu X, Lu H, Zhang X, Ma L, Gao R, Zhang Y. 2012. Real-time investigation of acute toxicity of ZnO nanoparticles on human lung epithelia with hopping probe ion conductance microscopy. *Chem. Res. Toxicol.* **25**: 297–304.

Youle RJ, Strasser A. 2008. The BCL-2 protein family: Opposing activities that mediate cell death. *Nat. Rev. Mol. Cell Biol.* **9**: 47–59.

Zhang Y, Jiang L, Jiang L, Geng C, Li L, Shao J, Zhong L. 2011. Possible involvement of oxidative stress in potassium bromate induced genotoxicity in human HepG2 cells. *Chem. Biol. Int.* **189**: 186–191.